ПРИКЛАДНАЯ МАТЕМАТИКА

UDC 621.318.132+537.622.4
MSC 65Z05

Magnetic model MMTC-2.2 of ITER tokamak complex

V. M. Amoskov[1], *A. V. Belov*[1], *V. A. Belyakov*[1,2], *E. I. Gapionok*[1], *Y. V. Gribov*[3], *V. P. Kukhtin*[1], *E. A. Lamzin*[1], *Y. Mita*[3], *A. D. Ovsyannikov*[2], *D. A. Ovsyannikov*[2], *L. Patisson*[3], *S. E. Sytchevsky*[1,2], *S. V. Zavadskiy*[2]

[1] JSC "NIIEFA", 3, Doroga na Metallostroy, St. Petersburg, 196641, Russian Federation
[2] St. Petersburg State University, 7–9, Universitetskaya nab., St. Petersburg, 199034, Russian Federation
[3] ITER Organization, Route de Vinon-sur-Verdon, CS 90 046, 13067, St. Paul Lez Durance Cedex, France

For citation: Amoskov V. M., Belov A. V., Belyakov V. A., Gapionok E. I., Gribov Y. V., Kukhtin V. P., Lamzin E. A., Mita Y., Ovsyannikov A. D., Ovsyannikov D. A., Patisson L., Sytchevsky S. E., Zavadskiy S. V. Magnetic model MMTC-2.2 of ITER tokamak complex. *Vestnik of Saint Petersburg University. Applied Mathematics. Computer Science. Control Processes*, 2019, vol. 15, iss. 1, pp. 5–21. https://doi.org/10.21638/11702/spbu10.2019.101

The stray poloidal magnetic field produced in ITER outside the tokamak is significantly higher than in any present machines. This magnetic field magnetizes the steel rebar reinforcing the building concrete structures enclosing the tokamak. As a result, reinforced structures of the ITER building may produce a substantial magnetic field with the axisymmetric component (toroidal mode number $n = 0$) affecting the plasma initiation and non-axisymmetric components ("error fields" with $n = 1; 2$) deteriorating plasma performance. This paper presents an upgraded Magnetic Model of the ITER Tokamak Complex, MMTC-2.2, for assessment of the stray field associated with the reinforced structures. This magnetic model MMTC-2.2 takes into account the CATIA models of the Tokamak Complex Buildings and volumetric fractions of steel for the rebar in the building structures as they were in the design in 2016.

Keywords: ITER, stray magnetic fields, error fields, steel magnetization.

Introduction. The ITER Tokamak Complex (Fig. 1 [1]) consists of the Tokamak and Tritium nuclear buildings and the Diagnostic building [2] located in a common pit (Fig. 2).

The tokamak itself is located in the bioshield pit of the main nuclear building *11*. A circular lid closes the bioshield from the top at the upper levels of the building (Fig. 2).

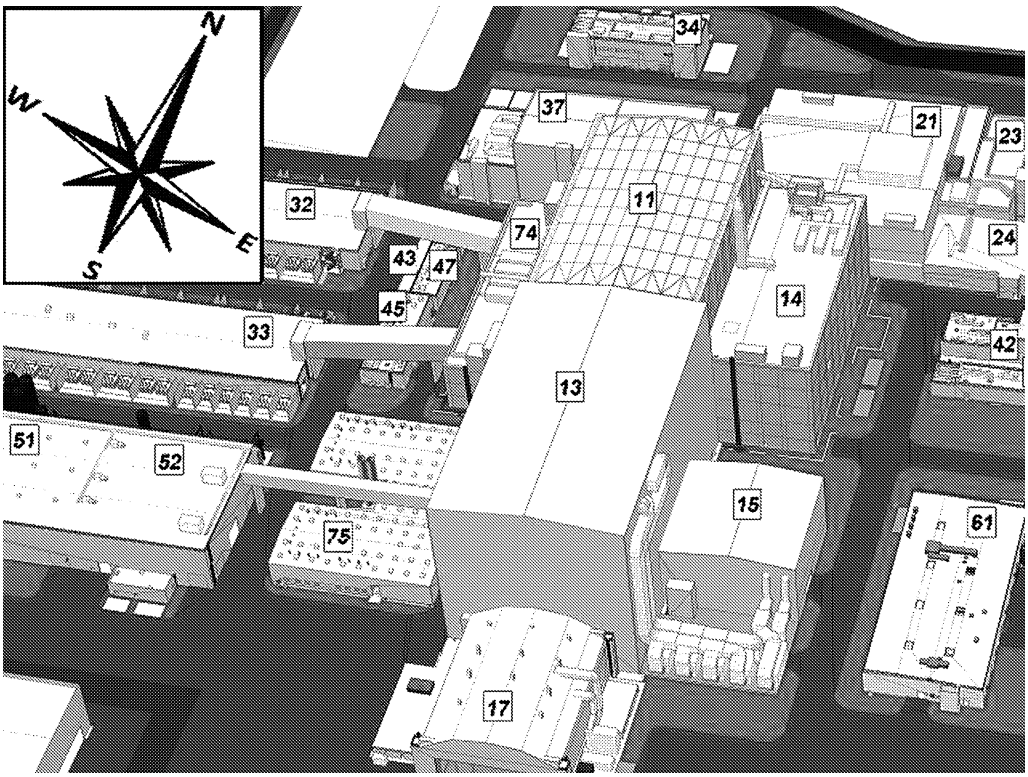

Figure 1. ITER site layout with Tokamak Complex (buildings *11*, *14*, *74*), Assembly Hall (*13*) and other auxiliary buildings

Most of the building structures of the ITER Tokamak Complex contain magnetic materials such as steel rebar in concrete. To assess the magnetic fields produced by concrete reinforced with steel rebar and, therefore, magnetized by the stray field of the tokamak, a simplified global magnetic model of the Tokamak Complex (MMTC-1) was proposed in [3]. The MMTC-1 was based on the preliminary design of the ITER Tokamak Complex. The model contained a restricted set of the global tokamak building structures described in [3]. The MMTC-1 was used for the assessment of the error fields associated with a global asymmetry of the tokamak complex [3] and stray fields outside [4] and inside [5] the Vacuum Vessel.

This paper describes an upgraded magnetic model of the Tokamak Complex, MMTC-2.2, which takes into account the data obtained with the use of the CATIA CAD/CAM multi-platform software suite [6] and the volumetric steel fractions in the building structures as they were in the design of Tokamak Complex buildings in 2016. The model MMTC-2.2 includes all the tokamak building structures and the Excavation seismic pit and, therefore, can be considered as a complete magnetic model of the Tokamak Complex. For this reason, the model MMTC-1 appears to be obsolete, and preliminary evaluations in [3–5] should be renewed. Corresponding results will be presented elsewhere.

The Tokamak General Coordinate System (TGCS) was used in this study.

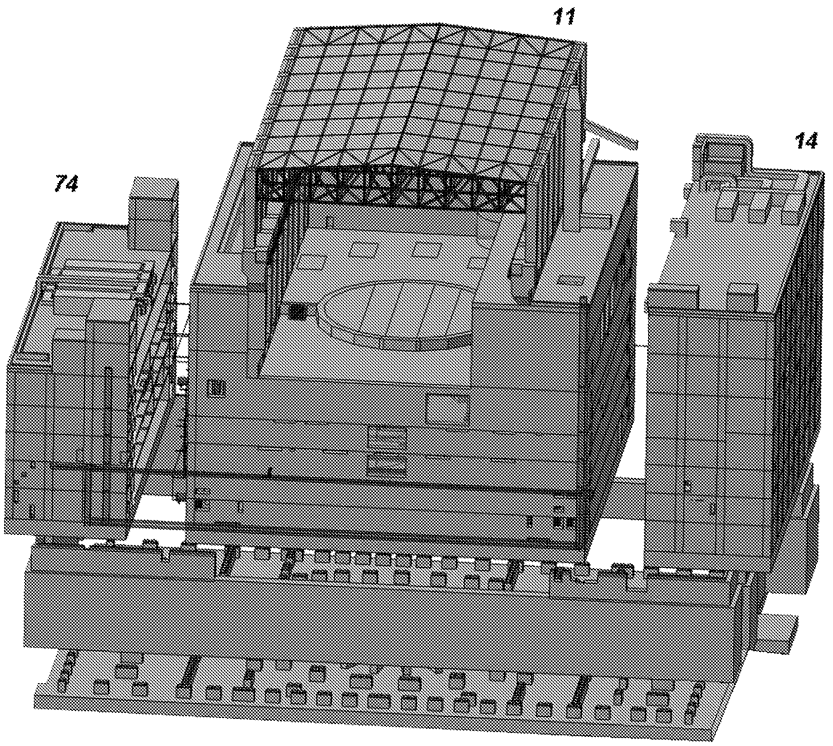

Figure 2. Exploded view of Tokamak Complex buildings located in excavation pit
11 — tokamak building; *14* — diagnostic building; *74* — tritium building.

Calculation of magnetic field. The anticipated field is simulated with the code KLONDIKE [7, 8] utilizing the integral formulation of the magnetic field problem [9–11] in terms of the magnetization vector. The magnetization distribution is calculated as a self-consistent problem implemented with the code as described below.

The magnetic field strength at an observation point $\mathbf{a}$ produced by a magnetic material with magnetization $\mathbf{M}$ and volume dV located at the point $\mathbf{r}$ is determined as [12, 13]

$$d\mathbf{H}(\mathbf{a}) = -\frac{dV}{4\pi}\nabla_{\mathbf{a}}\frac{(\mathbf{M}\cdot(\mathbf{a}-\mathbf{r}))}{|\mathbf{a}-\mathbf{r}|^3}, \tag{1}$$

where in the Cartesian coordinates $\nabla_{\mathbf{a}} = \frac{\partial}{\partial x_{\mathbf{a}}}\mathbf{e}_1 + \frac{\partial}{\partial y_{\mathbf{a}}}\mathbf{e}_2 + \frac{\partial}{\partial z_{\mathbf{a}}}\mathbf{e}_3$, here $\mathbf{e}_1$, $\mathbf{e}_2$, $\mathbf{e}_3$ are the orts of the coordinate system.

Thus, spatial derivation in equation (1) is made at a constant radius-vector $\mathbf{r}$ for the point, where the magnetized volume dV is located.

The field generated by magnetized volume V is determined as

$$\mathbf{H}(\mathbf{a}) = -\frac{1}{4\pi}\int\limits_V \nabla_{\mathbf{a}}\frac{\mathbf{M}(\mathbf{a}-\mathbf{r})}{|\mathbf{a}-\mathbf{r}|^3}dV.$$

Assuming a uniform magnetization, we obtain

$$\mathbf{H}(\mathbf{a}) = \frac{1}{4\pi}\int\limits_S \frac{\mathbf{M}(\mathbf{a}-\mathbf{r})}{|\mathbf{a}-\mathbf{r}|^3}d\mathbf{S} = \frac{1}{4\pi}\sum_{i=1}^{3} M_i \int\limits_S \frac{a_i - r_i}{|\mathbf{a}-\mathbf{r}|^3}d\mathbf{S}, \tag{2}$$

where S is the surface bounding the volume V; M_i, a_i, r_i $(i = 1, 2, 3)$ are respective vector components. Mathematically, formula (2) is equivalent to the matrix equation

$$\mathbf{H}(\mathbf{a}) = \mathbf{A} \cdot \mathbf{M},$$

here $\mathbf{M}$ is the constant magnetization vector in the volume V; the matrix $\mathbf{A}$ is expressed as

$$A_{ij} = \frac{1}{4\pi} \int\limits_S \frac{a_i - r_i}{|\mathbf{a} - \mathbf{r}|^3} (\mathbf{e}_j \cdot d\mathbf{S}). \tag{3}$$

If volume V is bounded with flat faces, the matrix coefficients A_{ij} can be found analytically.

In a magnetic medium

$$\mathbf{M} = \mathbf{F}(\mathbf{H}). \tag{4}$$

In (4) $\mathbf{M}(\mathbf{H})$ is the material equation presenting, in general case, the magnetization $\mathbf{M}$ as a known nonlinear function of the total magnetic field $\mathbf{H}$. For non-retentive isotropic materials $\mathbf{M} = (\mu(H) - 1)\mathbf{H}$, here $\mu(H)$ is the magnetic permeability, $H = |\mathbf{H}|$.

To calculate the field we apply a volume integral equation (VIE) method. The volume V with a magnetic material is assumed to be comprised of N uniformly magnetized domains V_k such that $V = \bigcup_{k=1}^{N} V_k$ and $V_i \bigcap V_j = 0$ for all $i \neq j$.

Assume that equation 6 is given for every domain V_k. Then, for any V_k we can write a system of nonlinear algebraic equations in terms of magnetization $\mathbf{M}$:

$$\begin{cases} \mathbf{H}_{tot} = \mathbf{A} \cdot \mathbf{M} + \mathbf{H}_{ext}, \\ \mathbf{M} = \mathbf{F}(\mathbf{H}_{tot}), \end{cases} \tag{5}$$

where $\mathbf{A}$ is the (3×3) influence matrix of the components of $\mathbf{M}$ associated with the domain V_k in formula (3); $\mathbf{H}_{ext}$ is the external field with respect to V_k; $\mathbf{H}_{tot}$ is the total field in the centre of V_k.

The system (5) is solved through a simple iteration procedure [14, 15]:

$$\mathbf{M}^{(n+1)} = \mathbf{M}^{(n)} + \alpha \left(\mathbf{F}(\mathbf{A}\mathbf{M}^{(n)} + \mathbf{H}_{ext}) - \mathbf{M}^{(n)} \right),$$

here $\mathbf{M}^{(n)}$ and $\mathbf{M}^{(n+1)}$ are, respectively, magnetization obtained in successive iterations, α is the iteration parameter. A higher convergence rate can be achieved with the use of the BT process [16] of the iterative acceleration thus making computations more time-effective.

To stop the iterative solution, the following criterion is applied:

$$\left| \mathbf{F}(\mathbf{A}\mathbf{M}^{(n)} + \mathbf{H}_{ext}) - \mathbf{M}^{(n)} \right| \leqslant \delta \left| \mathbf{M}^{(n)} \right| + \varepsilon,$$

where δ and ε are the relative and absolute accuracy of the solution, respectively.

Magnetic model of tokamak building. Calculation results. As shown [17, 18], a required engineering accuracy of a few percent for field evaluation with regard to the effect of steel rebar reinforcement can be largely provided with an isotropic model described below.

The tokamak building consists of five machine levels B2, B1, L1, L2, L3, two upper levels L4, L5 and two roof levels R1, R2 (Fig. 3).

The accepted tokamak complex sectioning (Fig. 4) correspond to regions with different steel fractions. The area related to the tokamak building is marked white. The building center is sectioned with concentric circles with the following outer radii: $R_1 = 8.94$ m for the section S1, $R_2 = 12.08$ m for the section S2, $R_3 = 18.4$ m for the section S3, $R_4 = 29.69$ m for the section S4.

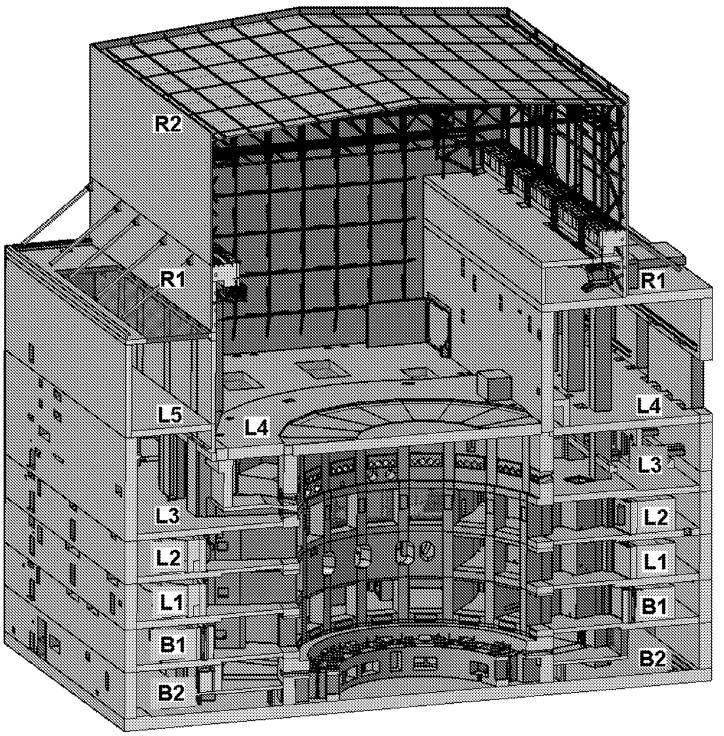

Figure 3. Cross-section of tokamak building *11* for levels B2–R2

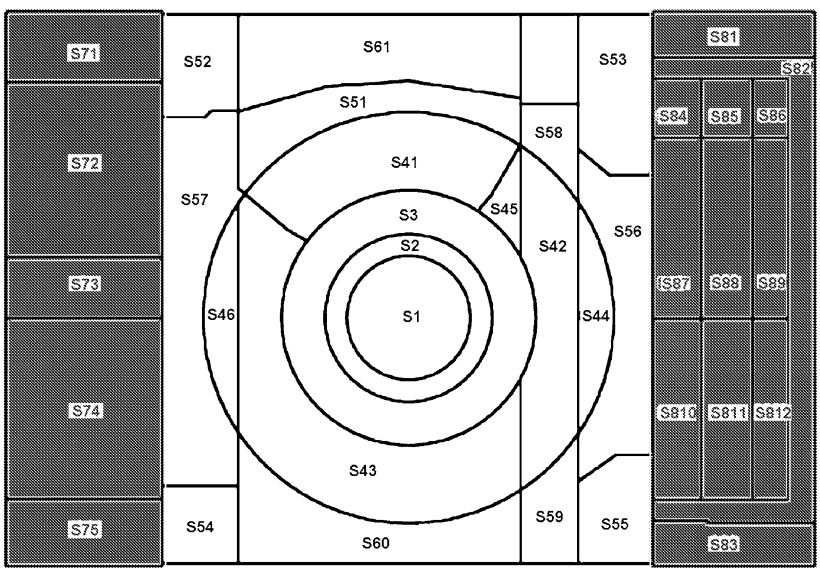

Figure 4. Tokamak complex sections (area inside tokamak building is marked white)

The floor slabs B2, B1, L1, L2, L3 are located at $Z = -13.08$, -6.73, -1.48, 3.9, and 9.08 m in TGCS, respectively.

Each level B2–L3 (Fig. 5, *a*–*e*) includes the slab (pos. *1*), bioshield walls (*2*),

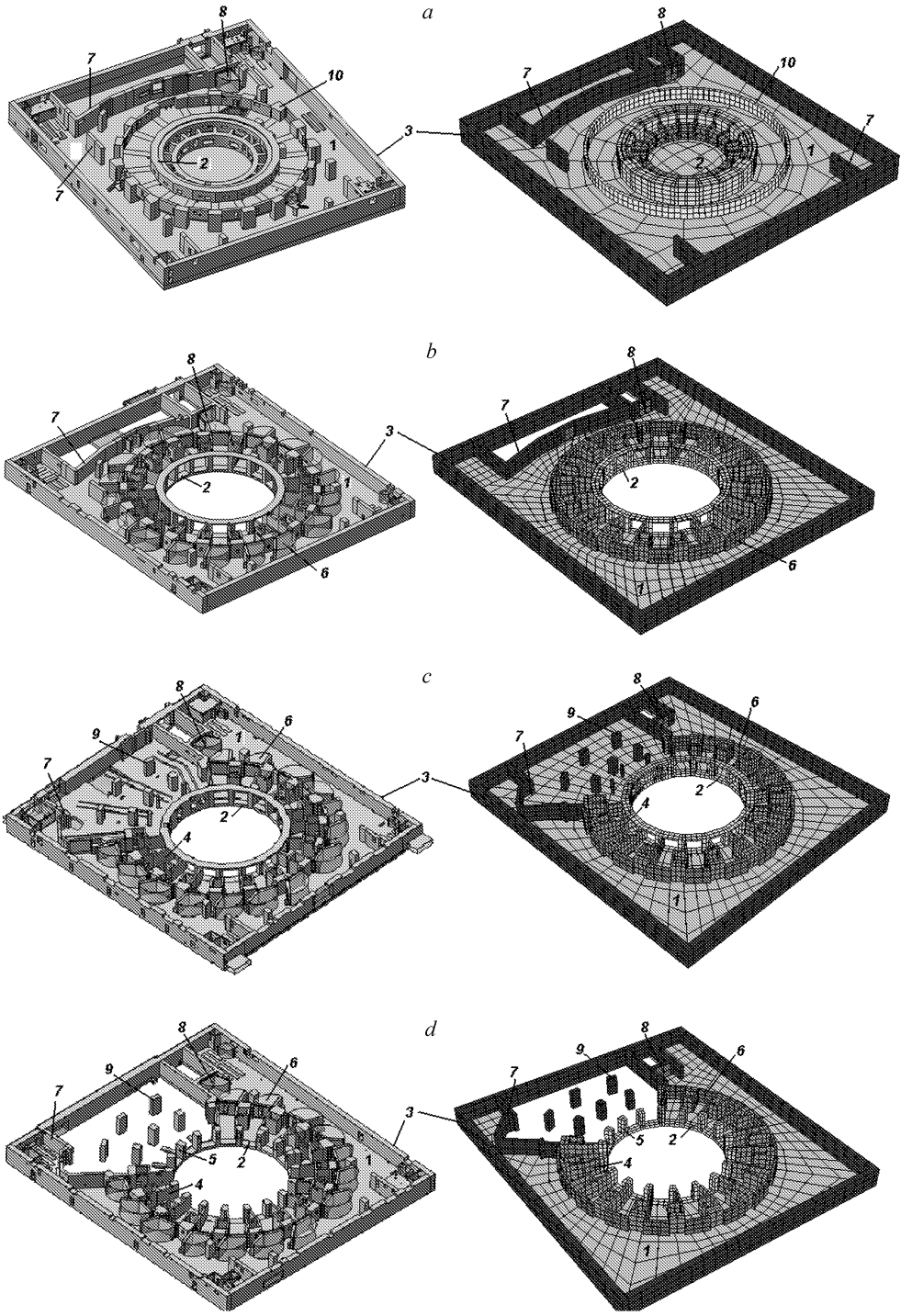
a
b
c
d

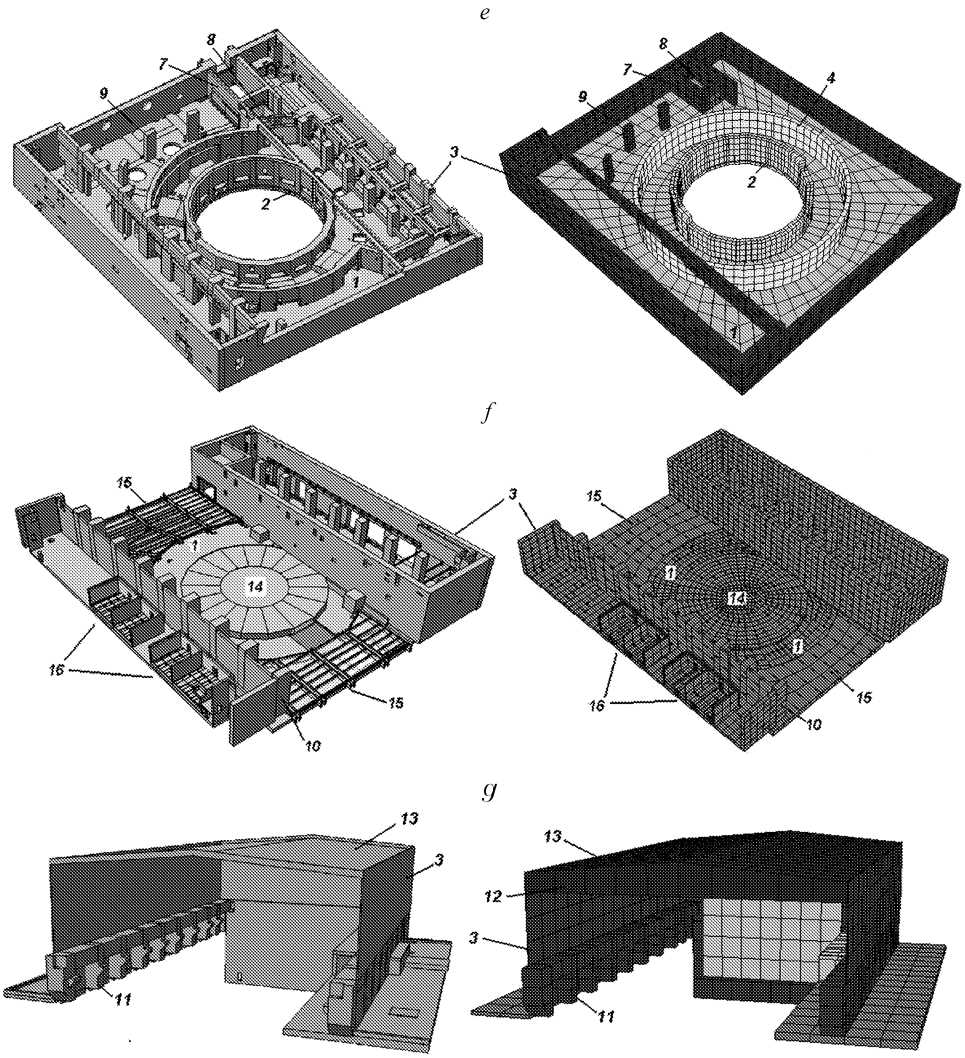

Figure 5. CATIA (in left) and KLONDIKE (in right) model of levels B2 (*a*), B1 (*b*), L1 (*c*), L2 (*d*), L3 (*e*), L4–L5 (*f*), R1–R2 (*g*)

Numbered structures are: slabs (*1*), bioshield walls (*2*), external walls (*3*), internal port cell walls (*4*), central zone columns (*5*), port cell doors (*6*), internal walls (*7*), cargo lift doors (*8*), internal separate columns (*9*), cryostat support (*10*), overhanging columns (*11*), steel trussworks (*12*), roof (*13*), bioshield lid (*14*), shielding platforms and supporting beam structures (*15*), SIC rooms (*16*) (one wall is omitted for the SIC rooms view).

external walls of the tokamak building (*3*), internal port cell walls (*4*), central zone columns (*5*, if any), port cell doors (*6*), internal walls (*7*) with cargo lift doors (*8*), and internal separate columns (*9*, if any). At each level the doors at the port cell walls are made of steel with a thickness of 0.782 m. The thickness of the cargo lift doors mounted into the internal walls is 0.153 m. The levels L4–R2 (Fig. 5, *f*, *g*) form the upper levels of the building up to the roof.

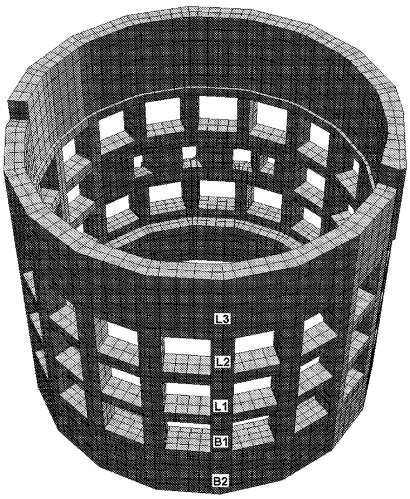

Figure 6. Computational model of central part of tokamak building (bioshield) at levels B2–L3

The concrete bioshield (Fig. 6) has been modeled using its realistic geometry, as a 18-hedron structure which located within the ring S3 (see Fig. 4) in the central part of the tokamak building. As seen from Fig. 5, *b*–*d*, the bioshield has openings at the levels B1–L2 for connection with the lower, equatorial, and upper ports of the ITER vacuum vessel.

A detailed description of each level is given in the Appendix A.

In the finalized computational model MMTC-2.2 (Fig. 7) the tokamak building structures are represented via a set of uniformly magnetized volume elements ("bricks"). The magnetization distribution is found self-consistently as described in the previous section. Then the stray field from MMTC-2.2 at any point is a sum of fields from all magnetized bricks.

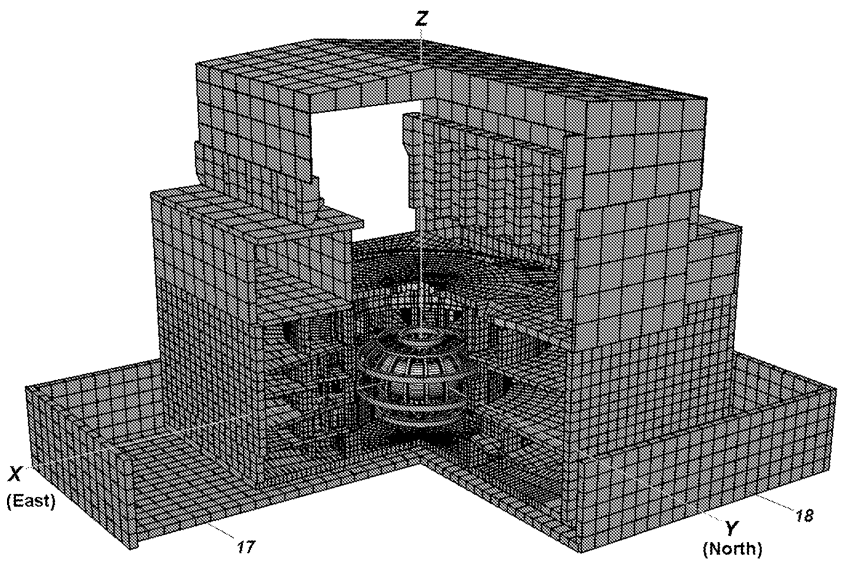

Figure 7. Computational 3D model of tokamak building (MMTC-2.2) including the machine in TGCS (a fourth of model is removed)
17 — seismic isolation basemat; *18* — excavation support structure walls.

A comparison and cross-checking computations on model validation are presented in [17–19]. Being calculated on the base of analytical expressions, the field as the "Maxwell" one simulated with the code KLONDIKE is smooth by definition.

In similar models (MMTC-1 [3], MMTC-2.2) the lattice of steel bars is replaced by an equivalent homogeneous isotropic materials with magnetic properties described by the dependence of magnetic induction $B = 0.5k \cdot f(H)$ on the field strength H. Here $f(H)$ is the magnetization curve of the reinforcement [20] and k is the volumetric filling

factor of concrete with reinforcement. Coefficient 0.5 is the effective filling factor for the typical placement of bars in two mutually perpendicular directions [17], in which 50 % of reinforcement bars can effectively conduct the magnetic flux of the external field oriented along the bars. This occurs when the field is parallel to the plane of the bar lattice. In the perpendicular direction to this plane there are no bars to conduct effectively the magnetic flux. As the consequence, the magnetization in the perpendicular direction must be weak, and the effect of the corresponding field component manifests relatively weakly [17, 18].

Figure 8 presents a simulated field map produced by the magnetized steel structures of the tokamak building only at the End-Of-Burn (EOB) state of the representative 15 MA DT scenario, when the stray field of the tokamak is maximal. The total stray field around the machine is presented in Fig. 9.

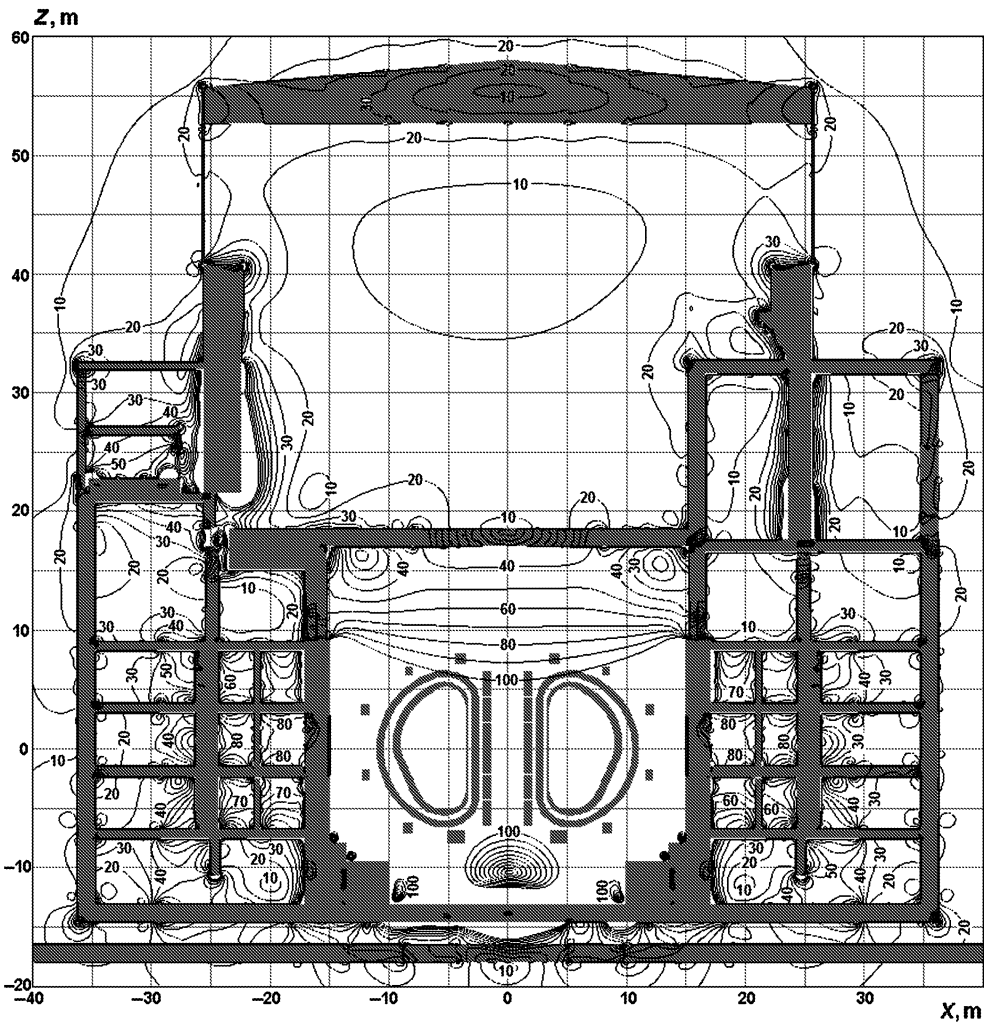

Figure 8. Field (in Gauss) produced by magnetized structures of tokamak building only at EOB of representative 15 MA DT plasma scenario in vertical cross-section $Y = 0$ of TGCS

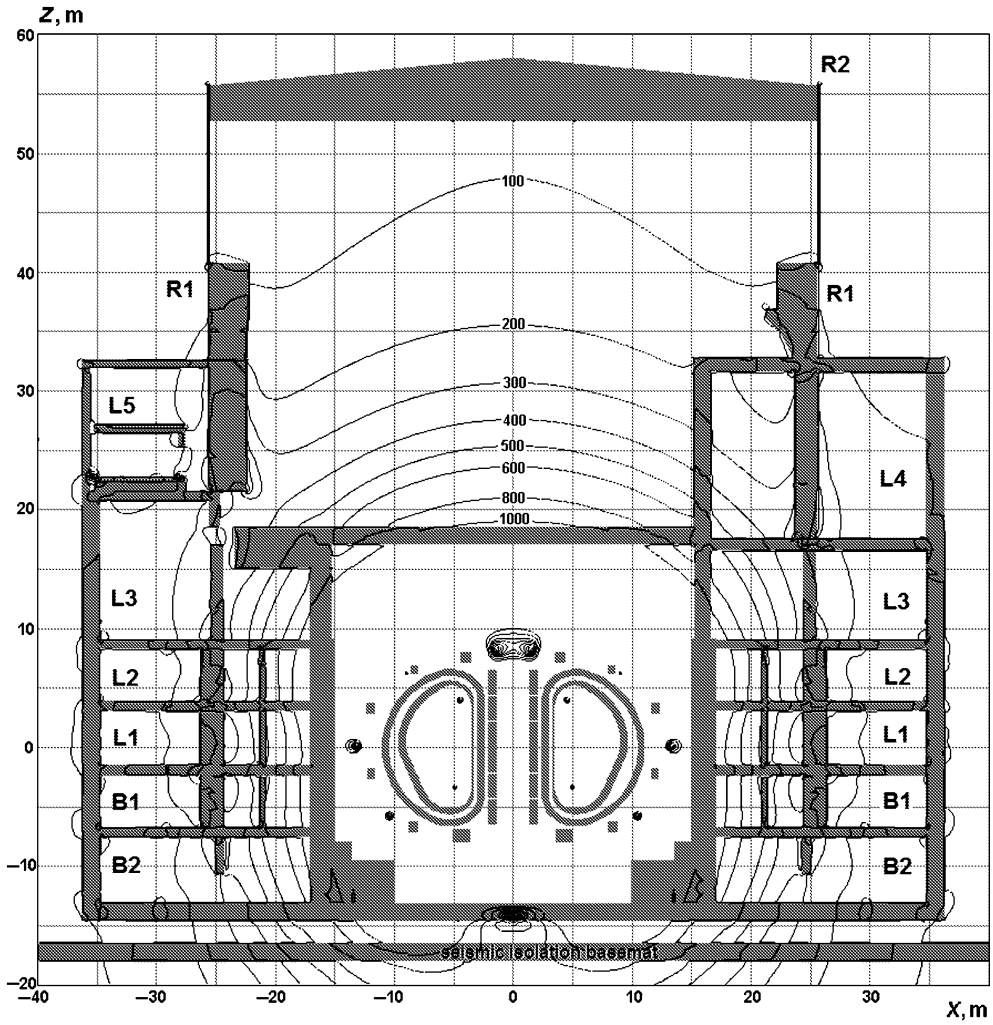

Figure 9. Total field (in Gauss) produced by ITER PF system, plasma and MMTC-2.2 at EOB of representative 15 MA DT scenario in vertical cross-section $Y = 0$ of TGCS

Conclusions. The detailed magnetic model MMTC-2.2 of the ITER tokamak complex has been developed that reflects the design of the tokamak building and volumetric fractions of the steel reinforcement as they were in 2016. The model includes the excavation support structures and all the building levels B2–R2 up to the roof and can be considered as a complete magnetic model of the tokamak building. The model describes in detail the slabs, bioshield, external and internal walls, internal port cell walls, columns and steel doors at every level.

Developed in the frame of the integral approach, the model allows us easily to take into account additional structures (for example, the magnetic field reduction systems of injectors) and their magnetic effect.

Using MMTC-2.2, the magnetic field produced by the ITER PF system, plasma and magnetized steel structures of the tokamak complex has been calculated for the EOB state of the representative 15 MA DT scenario. The simulated field maps are presented in the

central cross-section of the tokamak building, that can be used for first estimation of the magnetic field around the machine.

The MMTC-2.2 itself and the simulated fields of the tokamak building are planned to be applied for a series of related problems:

– correction of scenario of PF system operation to provide the plasma breakdown conditions;

– assessment of error fields produced by magnetized steel structures;

– calculation of magnetic fields for assessment of functionality of magnetic-sensitive equipment;

– evaluation of magnetic forces acting on building structures, etc.

These studies are under progress now.

Disclaimer: *ITER is a Nuclear Facility INB-174. The views and opinions expressed herein do not necessarily reflect those of the ITER Organization.*

Appendix A. Detailed description of the levels B2–R2

A.1. Level B2 (the lowest level)

B2 level slab. The B2 level slab (see Fig. 5, *a*, pos. *1*) is a concrete plate with the dimensions of 72.5 m in the north-south direction and 80.8 m in the east–west direction. The slab thickness is 1.5 m. The volumetric fractions of steel rebar for the sections S1, S2, and S3 (see Fig. 4) are 6.87, 8.38 and 6.02 %, respectively. An average volumetric fraction of steel rebar at the subsections S41–S46 (see Fig. 4) has been assessed as 4.77 % for the common section S4. An average volumetric fraction of steel rebar for the rest has been evaluated as 2.34 %.

B2 level bioshield. The concrete bioshield is an 18-hedron structure (see Fig. 6) located within the section S3 (see Fig. 4) in the central part of the tokamak building. The bioshield thickness at the level B2 is 3.25 m. The volumetric fraction of steel rebar at this level is 4.5 %. The bioshield has been modeled as three solid trapezoids in every 1/18 part of the 18-hedron structure in order to simulate in details the curvature of the bioshield in the toroidal direction.

B2 level port cell walls. The port cell walls at the level B2 form a concrete cylinder with a thickness of 0.8 m. There are no steel doors at this level, according to the ITER design. An average volumetric fraction of steel rebar for the walls is taken as 2.74 %.

B2 level external walls. The wall height for the level B2 is 5.55 m. The volumetric fractions of steel rebar for the north, west, south, and east walls at the level B2 are, correspondingly, 2.49, 2.55, 2.45 and 2.03 %.

B2 level cryostat support. The cryostat support is a cylindrical structure located in section S2. The cylinder wall is 1.5 m thick with a volumetric steel fraction of 8.27 %. Between the support and the bioshield, vertical stiffening crosswalls are placed radially with a 20-degree step. Every crosswall is 1 m thick with a volumetric steel fraction of 12.3 %.

B2 level internal walls. A set of internal walls placed at the level external regions has been added to the model. The wall steel fractions are in the range from 1.4 to 3.4 %. The door on the wall is 100 % steel.

A.2. Level B1

B1 level slab. The slab thickness is 0.8 m (see Fig. 5, *b*, pos. *1*). Within the subsections S41–S46 (see Fig. 4) the volumetric fraction of steel rebar is evaluated in the range from 4.27 to 4.62 %. At the slab periphery the volumetric fraction of steel rebar varies in the range from 1.9 to 3.88 %.

B1 level bioshield. The bioshield at the level B1 is a regular polyhedron structure

with 18 sides and rectangular openings. Each regular sector of the bioshield consists of four components: two vertical columns and two horizontal plates. The volumetric steel fractions for the vertical components are equal to 5.35 %. The volumetric steel fractions of the upper and lower plates correspond to those of the section S3 (see Fig. 4) of the slab central zones at the levels B1 and L1, i. e. 5.21 and 7.06 %, respectively.

B1 level port cell walls and doors. The port cell walls and doors at the level B1 form a regular structure. A regular sector (1/18) includes walls, columns and one steel door. The volumetric fractions of the components are evaluated in the range from 3.14 to 5.44 % and 100 % for steel doors.

B1 level external walls. The wall height for the level B1 is 5.15 m. The volumetric fraction of the north, west, south, and east walls for the level B1 are, correspondingly, 2.9, 2.2, 1.9 and 2.1 %.

B1 level internal walls. B1 internal walls are located at the level periphery mostly near the slab opening. The volumetric steel fractions of the walls vary in the range from 1.8 to 4.1 %. The doors are 100 % steel.

A.3. Level L1

The main peculiarity of level L1 (see Fig. 5, *c*) is the presence of the Diagnostic (DNBI) and Heating Neutral Beam Injectors (HNBIs). So, the bioshield is designed to fit openings for the vacuum vessel (VV) equatorial ports, including the VV injector ports. Also, the area near the injectors is free from port cell walls.

L1 level slab. The L1 slab thickness is 0.9 m. The slab has been modeled via hexahedral segments. The slab model takes into account the slab opening at the north side. Within the subsections S41–S46 (see Fig. 4) the volumetric fraction of steel rebar is evaluated in the range from 3.1 to 4.6 %. At the slab periphery the volumetric fraction of steel rebar varies in the range from 1.7 to 4.2 %.

L1 level bioshield. The bioshield at the level L1 consists of a set of regular sectors and three injector sectors. The volumetric fractions of steel rebar vary in the range from 2.0 to 7.1 %.

L1 level port cell walls and doors. A 20-degree sector of the cell walls and doors as a local model has been rotated in the toroidal direction to produce a 260-degree regular structure. The volumetric fractions of steel rebar vary in the range from 2.1 to 5.5 %. The doors are 100 % steel.

L1 level external walls. The wall height for the level L1 is 5.48 m. The volumetric fraction of the north, west, south, and east walls for the level L1 are, correspondingly, 1.9, 1.9, 3.5 and 2.2 %.

L1 level internal walls, doors and columns. Internal walls have been introduced in the model. The walls connect the northern external wall of the building and the port cell walls. The volumetric steel fractions for the internal walls vary in the range from 1.1 to 4.5 %.

Three radial rows of three columns each are located between NBIs at the northern side of level L1. The volumetric steel fractions of columns in a row vary as 1.6, 2.2 and 1.1 % in the radial direction.

A.4. Level L2

The level L2 (see Fig. 5, *d*) correlates with the level of the VV upper ports.

L2 level slab. A part of the L2 level slab is absent due to the presence of the injectors at the levels L1 and L2. The slab thickness is equal to 0.8 m.

The slab can be conditionally divided into two major parts: the inner circle covering subsections S41–S46, and the periphery formed by the rest slab subsections. An average

volumetric steel fraction is evaluated as 4.2 % for the inner circle and 2.0 % for the periphery.

L2 level bioshield. The volumetric steel fractions of the columns and plates of the bioshield are equal to 7.5 and 6.9 %, respectively.

L2 level port cell walls and doors. A 20-degree regular sector consists of steel door (volumetric fraction 100 %), columns (2.6 %) and separate parts of the walls with a common volumetric steel fraction of 4.1 %.

L2 level external walls. The wall height for the level L2 is 5.18 m. The volumetric steel fraction of the north, west, south, and east walls for the level L2 are, correspondingly, 2.9, 1.9, 1.9 and 1.85 %.

L2 level internal walls, doors and columns. Internal walls are introduced in the model at the level L2. The walls surround the floor hole for the H/DNB injectors, located at the level L1. The volumetric steel fractions vary in the range from 1.2 to 4.0 %. The door on the wall is 100 % steel.

The L1–L2 columns located surrounding the H/DNB injectors have a volumetric steel fraction of 2.6 %.

A.5. Level L3

The level L3 (see Fig. 5, *e*) correlates with the upper level of the machine (the top of the cryostat), therefore no access to the ports is needed.

L3 level slab. The slab thickness is 0.8 m. The L3 slab has been updated in order to take into consideration the slab opening at the region of the northern external wall. For the inner circle the volumetric steel fractions are of 6.4 % (northern part) and 3.7 % (rest part of the ring), for the slab periphery — 4.5 % (northern part), 2.0 % (for the rest).

L3 level bioshield. The bioshield height at level L3 varies from 6 to 8 m, if measured from the L3 level slab, due to its connection to the bioshield lid counterpart. The thickness of the bioshield at the level L3 is 1.65 m.

The volumetric steel fraction of the bioshield located in section S3 (see Fig. 4) has been taken as 3.9 % above the slab and 6.1 % for its part coinciding with the L3 level slab.

L3 level cell walls. A cell wall structure has been simplified to a cylinder with a thickness of 1.15 m. The volumetric steel fraction of 2.9 % is taken as an average value for the walls located in section S4 (see Fig. 4).

L3 level external walls. The external wall height for the level L3 varies in the range from 7.8 to 12.5 m. The volumetric steel fraction of the north, west, south, and east walls for the level L3 are, correspondingly, 2.2, 2.1, 2.1 and 2.1 %.

L3 internal walls and columns. The internal wall is parallel to the western external wall over the entire level L3 and has the volumetric steel fraction of 2.4 %.

The internal walls have also been added around a vertical passageway near the northern external wall. The volumetric steel fraction of the walls is 2.0 %, the door is 100 % steel. The volumetric steel fraction for columns is 2.1 %.

A.6. Level L4

L4 level slab and bioshield lid. The L4 level slab (see Fig. 5, *f*, pos. *1*) is 1 m thick. At this level the separate slab parts differ in height of about 2 m.

The volumetric fraction of steel rebar in the slab has been estimated as its maximal value of 2.7 % for the elevated part and 2.9 % for the rest.

The bioshield lid (*14*) is represented as an 18-hedral structure positioned in section S3, with a thickness of 1.4 m and a volumetric steel fraction of 4.3 %.

L4 level shielding platforms. The northern and southern shielding platforms, located

near the bioshield lid (*15*), are steel frames 20 mm thick each. For the northern shielding platform the volumetric steel fraction is 2.5 %, for the southern shielding platform — 3.2 %.

The shielding platforms are mounted above the floor on steel trussworks. The trussworks have been modeled as hexahedra with the steel fraction taken as a ratio of the trusswork volume to the hexahedron volume.

L4 level external wall. The L4 level external walls (pos. *3*) form a rectangular structure located at the east side of the tokamak building. The wall thickness is 1.5 m.

The volumetric steel fractions are equal to 2.1 % for the northern and eastern walls, 2.2 % for the southern, and 3.0 % for the western walls.

A.7. Levels L5–R2

L5 level. The L5 level (see Fig. 5, *f*) is represented as a set of closed premises, located at the western part of the tokamak building. They occupy the subsections S52, S57, S54 and partially subsections S46, S51, S61 and S60 (see Fig. 4). The level includes the slab (pos. *1*), walls (*3*) and overhanging columns (*10*).

The slab thickness is 0.8 m. The volumetric steel fraction for the slab is 2.7 %.

The thickness of the walls varies in the range from 0.75 to 1 m. The volumetric steel fractions for the northern, southern, western and eastern walls at the level L5 are equal to 2.0, 2.1, 2.1 and 3.0 %, correspondingly.

The SIC rooms shown in Fig. 5, *f* (pos. *16*) are also the structures of level L5. Steel plates with a thickness of 30 mm are located at the bottom of the SIC rooms and supported by beams. The volumetric steel fraction is 2.8 % for the SIC room ceiling and walls and 2.0 % for the BHDPE ceiling and walls. The SIC room neutronic insulation from the bottom has the volumetric steel fraction equal to 2.1 %.

R1 level. The R1 level (see Fig. 5, *g*) includes separate parts of the slab, positioned in the eastern and western parts of the building, the northern wall, the overhanging columns and closed auxiliary rooms in the north-east part of the building.

The thickness of the northern wall is 0.75 m. The volumetric steel fraction for the northern wall (taking into account the fabricated metals fixed at the wall) is estimated as 3.2 %. The thickness of the eastern and western parts of slab is 1.2 and 0.6 m, correspondingly. The volumetric steel fraction is equal to 2.0 and 2.7 %, respectively.

The filling factor for the columns (see Fig. 5, *g*, pos. *11*) is taken as 4 %.

The volumetric fractions of steel rebar for separate structures of auxiliary rooms are evaluated in the range from 2.0 to 2.1 %.

R2 level. The R2 level includes side (eastern and western) and rear (northern) walls (see Fig. 5, *g*, pos. *3*) as well as the roof (*13*) with a system of the trussworks (*12*) and stiffness ribs. The thickness of the roof and walls is 0.18 m.

The volume of steel trussworks placed under the roof has been estimated as 34.42 m^3, while the region occupied by trussworks has a volume of 17353 m^3. So, in the model the volumetric steel fraction of solids for this region is taken as 0.2 %.

For the northern wall the volumetric steel fraction is about 1 %.

For every side wall the volumetric steel fraction is evaluated as 7 %.

A.8. Excavation support structures

Excavation support structures envelop all the three buildings of the tokamak complex on a ground level (see Figs 2, 7).

Seismic isolation basemat (slab). The seismic isolation basemat is a plate made of concrete with steel rebar with a dimension of 84.8 m in the north-south direction and 120.6 m in the east-west direction. The basemat thickness is 1.5 m. Anti-seismic bearings are omitted in this model. The volumetric fraction of steel rebar is 2 %.

Excavation support structure walls. Dimensions of the inner array are 84.8 m in the north-south direction and 120.6 m in the east-west direction. The thickness of the external wall of the pit varies from 0.5 to 1.5 m downward. In the model the maximal thickness of 1.5 m has been taken. The wall height is 16.35 m. The lower portion of the northern wall has a thickness of 1.25 m. The volumetric fraction of steel rebar for the walls is 1.6 %.

Excavation support structures are seen at the bottom of Fig. 7. A room is made in the pit for the buildings *74* and *14* (see Fig. 2) omitted in MMTC-2.2.

References

1. ITER Tokamak Complex. URL: http://www.iter.org (accessed: 09.02.2018).

2. Cordier J.-J., Bak J.-S., Baudry A., Benchikhoune M., Carafa L., Chiocchio S., Darbour R., Elbez J., di Giuseppe G., Iwata Y., Jeannoutot T., Kotamaki M., Kuehn I., Lee A., Levesy B., Orlandi S., Packer R., Patisson L., Reich J., Rigoni G., Sweeney S. Overview of the ITER Tokamak Complex building and integration of plant systems toward construction. *Fusion Eng. Des.*, 2015, vol. 90, pp. 240–243.

3. Amoskov V., Belov A., Belyakov V., Gribov Y., Kukhtin V., Lamzin E., Maximenkova N., Sytchevsky S. Assessment of error field from ferromagnetic surrounding of ITER tokamak: ferromagnetic rebar of Tokamak Complex building. *Plasma Devices Oper.*, 2008, vol. 16, no. 4, pp. 225–233.

4. Amoskov V., Belov A., Belyakov V., Gribov Y., Kavin A., Kukhtin V., Lamzin E., Lobanov K., Maximenkova N., Mineev A., Sytchevsky S. Stray magnetic field at plasma initiation produced by ferromagnetic elements of the ITER Tokamak Complex. *Plasma Devices Oper.*, 2009, vol. 17, no. 4, pp. 238–249.

5. Amoskov V., Belov A., Belyakov V., Gribov Y., Kukhtin V., Lamzin E., Maximenkova N., Sytchevsky S. Stray magnetic field produced by ITER Tokamak Complex. *Plasma Devices Oper.*, 2009, vol. 17, no. 4, pp. 230–237.

6. CATIA CAD/CAM multi-platform. URL: https://www.3ds.com/products-services/catia/ (accessed: 09.02.2018).

7. Amoskov V., Belov A., Kashikhin V., Kukhtin V., Lamzin E., Severgin Yu., Shatil N., Sytchevsky S. Numerical simulation of 3D field of system using permanent magnets. *Proc. of Eur. Part. Accelerator Conference*. Barcelona, Spain, 1996, pp. 2161–2164.

8. Amoskov V. M., Belov A. V., Belyakov V. A., Belyakova T. F., Gribov Yu. A., Kukhtin V. P., Lamzin E. A., Sytchevsky S. E. Computation technology based on KOMPOT and KLONDIKE codes for magnetostatic simulations in tokamaks. *Plasma Devices Oper.*, 2008, vol. 16, pp. 89–103.

9. Tozoni O. V., Meyergoiz I. D. *Raschet trehmernyh elektromagnitnyh polei* [*Computation of spatial electromagnetic fields*]. Kiev, Tekhnika Publ., 1974, 352 p. (In Russian)

10. Akishin P. G., Sapozhnikov A. A. Metod obyomnyh integralnyh uravnenij v zadachah magnitostatiki [The volume integral equations method in magnetostatics problems]. *Vestnik of RUDN*, 2014, no. 2, pp. 310–315. (In Russian)

11. Akishin P. G., Vorozhtsov S. B., Zhidkov E. P. Calculation of the magnetic field of the isochronous cyclotron sector magnet by the integral equations method. *Proc. of COMPUMAG Conference*. Grenoble, 1978, JUNR-E9-11859.

12. Tamm I. *Fundamentals of the theory of electricity*. Moscow, Mir Publ., 1979. 695 p.

13. Thome R. J., Tarrh J. M. *MHD and fusion magnets: field and force design concepts*. New York, Wiley Publ., 1982, 249 p.

14. Kurbatov P. A., Arinchin S. A. *Chislennyi raschet elektromagnitnykh polei* [*Numerical calculation of electromagnetic fields*]. Moscow, Energoatomizdat Publ., 1984, 168 p. (In Russian)

15. Samarsky A. A., Nikolaev E. S. *Metody resheniya setochnykh uravneniy* [*Solution methods of finite-difference equations*]. Moscow, Nauka Publ., 1978, 592 p. (In Russian)

16. Fadeev D. K., Fadeeva V. N. *Vychislitelnye metody linejnoj algebry* [*Computation methods of linear algebra*]. Moscow, Fizmatgiz Publ., 1963, 734 p. (In Russian)

17. Amoskov V. M., Bazarov A. M., Belyakov V. A., Gapionok E. I., Kaparkova M. V., Kukhtin V. P., Lamzin E. A., Lyublin B. V., Sytchevsky S. E. Modelling of magnetic field perturbations in electrophysical devices due to the steel reinforcement of buildings. *Technical Physics*, 2017, vol. 62, no. 10, pp. 1466–1472.

18. Amoskov V., Bazarov A., Belyakov V., Gapionok E., Gribov Y., Kaparkova M., Kukhtin V., Lamzin E., Lyublin B., Ovsyannikov D., Sytchevsky S. Calculation of magnetic field from steel rebar of building with machine producing high stray field. *Fusion Eng. Des.*, 2018, vol. 135, pp. 165–173.

19. Amoskov V., Bazarov A., Kaparkova M., Kukhtin V., Lamzin E., Lyublin B., Belyakov V., Sytchevsky S., Gribov Y. Modeling magnetic effects of steel rebar of concrete surroundings for electrophysical apparatus. *Proceeding of RuPAC*, 2016, THPSC007, pp. 553–555.

20. El-Sherbiny M. Representation of the magnetization characteristic by a sum of exponentials. *IEEE Transactions on Magnetics*, 1973, vol. 9, no. 1, pp. 60–61.

21. *Multiobjective optimization library.* URL: http://home.ku.edu.tr/~moolibrary/ (accessed: 09.02.2018).

Received: November 18, 2018.
Accepted: December 18, 2018.

Author's information:

Victor M. Amoskov — PhD in Physics and Mathematics; sytch@sintez.niiefa.spb.su

Alexandr V. Belov — sytch@sintez.niiefa.spb.su

Valery A. Belyakov — Dr. Sci. in Physics and Mathematics, Professor; belyakov@sintez.niiefa.spb.su

Elena I. Gapionok — sytch@sintez.niiefa.spb.su

Yuri V. Gribov — PhD in Physics and Mathematics, Scientific Expert; Yuri.Gribov@iter.org

Vladimir P. Kukhtin — PhD in Physics and Mathematics; sytch@sintez.niiefa.spb.su

Evgeny A. Lamzin — Dr. Sci. in Physics and Mathematics; sytch@sintez.niiefa.spb.su

Yoshiyuki Mita — PhD; Yoshiyuki.Mita@iter.org

Alexandr D. Ovsyannikov — PhD in Physics and Mathematics, Assistant Professor; ovc74@mail.ru

Dmitrij A. Ovsyannikov — Dr. Sci. in Physics and Mathematics, Professor; dovs45@mail.ru

Laurent Patisson — PhD; Laurent.Patisson@iter.org

Sergey E. Sytchevsky — Dr. Sci. in Physics and Mathematics; sytch@sintez.niiefa.spb.su

Sergey V. Zavadskiy — PhD in Physics and Mathematics; svzav11@yandex.ru

Магнитная модель комплекса токамака ИТЭР ММТС-2.2

В. М. Амосков[1], *А. В. Белов*[1], *В. А. Беляков*[1,2], *Е. И. Гапионок*[1], *Ю. В. Грибов*[3], *В. П. Кухтин*[1], *Е. А. Ламзин*[1], *Е. Мита*[3], *А. Д. Овсянников*[2], *Д. А. Овсянников*[2], *Л. Патиссон*[3], *С. Е. Сычевский*[1,2], *С. В. Завадский*[2]

[1] АО «НИИЭФА», Российская Федерация, 196641, Санкт-Петербург, Дорога на Металлострой, 3
[2] Санкт-Петербургский государственный университет, Российская Федерация, 199034, Санкт-Петербург, Университетская наб., 7–9
[3] ITER Organization, Route de Vinon-sur-Verdon, CS 90 046, 13067, St. Paul Lez Durance Cedex, France

Для цитирования: *Amoskov V. M., Belov A. V., Belyakov V. A., Gapionok E. I., Gribov Y. V., Kukhtin V. P., Lamzin E. A., Mita Y., Ovsyannikov A. D., Ovsyannikov D. A., Patisson L., Sytchevsky S. E., Zavadskiy S. V.* Magnetic model MMTC-2.2 of ITER tokamak complex // Вестник Санкт-Петербургского университета. Прикладная математика. Информатика. Процессы управления. 2019. Т. 15. Вып. 1. С. 5–21. https://doi.org/10.21638/11702/spbu10.2019.101 (In English)

Полоидальные магнитные поля рассеяния, образующиеся снаружи токамака ITER, значительно более сильные, чем в любой другой существующей в настоящий момент установке. Они намагничивают арматуру, усиливающую бетонные конструкции здания. Ближайшая к плазме бетонная конструкция, биоэкран, в единицах малого радиуса плазмы расположена значительно ближе к плазме, чем бетонные стены зданий современных токамаков. В результате арматура бетонных конструкций здания ITER может продуцировать в области плазмы значительное магнитное поле с асимметричной компонентой (номер тороидальной моды $n = 0$), влияющее на образование плазмы,

и неосесимметричные компоненты (ошибки поля с $n = 1, 2$), воздействующие на поведение плазмы. Данная статья рассматривает усовершенствованную магнитную модель комплекса токамака ITER, ММТС-2.2, которая учитывает CATIA модели комплекса токамака и объемные коэффициенты заполнения стальной арматурой бетонных конструкций здания согласно последнему дизайну 2016 г.

Ключевые слова: ИТЭР, магнитные поля рассеяния, ошибка полей, намагниченность стали.

Контактная информация:

Амосков Виктор Михайлович — канд. физ.-мат. наук; sytch@sintez.niiefa.spb.su

Белов Александр Вячеславович — sytch@sintez.niiefa.spb.su

Беляков Валерий Аркадьевич — д-р физ.-мат. наук, проф.; belyakov@sintez.niiefa.spb.su

Гапионок Елена Игоревна — sytch@sintez.niiefa.spb.su

Грибов Юрий Владимирович — канд. физ.-мат. наук; Yuri.Gribov@iter.org

Кухтин Владимир Петрович — канд. физ.-мат. наук, ст. науч. сотр.; sytch@sintez.niiefa.spb.su

Ламзин Евгений Анатольевич — д-р физ.-мат. наук; sytch@sintez.niiefa.spb.su

Мита Ёшиюки — PhD; Yoshiyuki.Mita@iter.org

Овсянников Александр Дмитриевич — канд. физ.-мат. наук, доц.; ovc74@mail.ru

Овсянников Дмитрий Александрович — д-р физ.-мат. наук, проф.; dovs45@mail.ru

Лоран Патиссон — PhD; Laurent.Patisson@iter.org

Сычевский Сергей Евгеньевич — д-р физ.-мат. наук; sytch@sintez.niiefa.spb.su

Завадский Сергей Вячеславович — канд. физ.-мат. наук; svzav11@yandex.ru